

# Optical Superimposition of Infrared Thermography through Video Projection

Daisuke Iwai<sup>\*1</sup>, Kosuke Sato

Graduate School of Engineering Science, Osaka University  
1-3 Machikaneyama, Toyonaka, Osaka 560-8531, Japan

---

## Abstract

This paper presents a novel infrared thermography visualization technique where a sequence of captured thermal images is optically and simultaneously superimposed onto the target object via video projection in real time. In conventional thermography visualization, observers have to frequently move their eyes from the object to a 2D screen where a thermal image is displayed. In contrast, the heat distribution of the object's surface emerges directly onto its physical surface in the proposed method. As a result, the observer can intuitively understand the object's heat information just by looking at it in the real space. This paper explains the methods of geometric registration and radiometric compensation of the captured thermal image, which are required before video projection. Furthermore, several projection results are shown to validate the intuitiveness and usefulness of the proposed visualization method.

*Key words:* projection-based mixed reality, thermography visualization, intuitive visualization, nondestructive testing, medical diagnosis, surveillance

*PACS:* 07.05.Rm

---

## 1. Introduction and Motivation

Infrared (IR) thermography has been widely used in various applications such as medical diagnosis, non-destructive testing (NDT), and surveillance [1, 2]. In conventional thermography visualization, either a raw or superimposed thermal image of the target object is observed on a 2D screen. When the raw image is displayed, an observer has difficulty in identifying which part of the displayed thermal image corresponds to which part of the object's surface. Because the *object space*<sup>2</sup> and *display space*<sup>3</sup> are completely different, the observer must frequently move his (or her) eyes from the object to the screen in order to find geometric correspondences between the object and the displayed heat information (Fig. 1(a)).

Recently developed thermal imagers have additional built-in visible cameras each of which captures the target object from almost the same perspective as the IR

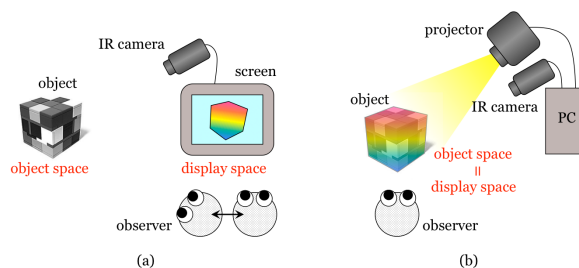


Figure 1: Diagrams of thermography visualization: (a) a conventional approach and (b) the proposed approach

camera. Note that we use the term “IR camera” to refer to either a Long-Wave infrared (LWIR) camera or a thermal camera in this paper. The captured thermal and visible images are registered and digitally superimposed on each other before being displayed on the screen. This enables the observer to intuitively find the aforementioned geometric correspondences on the screen. However, many thermography applications require the observer to comprehend the heat distribution on the physical object's surface rather than on the screen, except for remote surveillance. In these applications, the observer still has to frequently switch his (or her) focus from the object in real space to the displayed image on the screen,

---

<sup>\*</sup>Corresponding author.

Email address: daisuke.iwai@sys.es.osaka-u.ac.jp  
(Daisuke Iwai)

<sup>1</sup>Tel: +81(6)68506372, fax: +81(6)68506341

<sup>2</sup>A real 3D space where the target object exists

<sup>3</sup>A space where heat information is displayed

because the *object space* and the *display space* are still not the same.

There are three types of promising applications where it is particularly difficult to find geometric correspondences between a physical object and displayed information on a screen. The first is a scene where there is no geometric or radiometric distinctive feature, and thus no clue to the geometric correspondences. For instance, an observer might face difficulty in identifying the exact physical position of a roof leak when the ceiling has no texture on its surface. The second is a cluttered scene. Suppose that a scene is covered with many similar objects one of which has an unusually high temperature and has to be removed immediately. Although an observer who watches a thermal image of the scene could recognize the unusual situation, he might have difficulty in finding the one which has the high temperature. A diagnosis of a power distribution board can be considered an example of this case. The last is a moving object whose heat observation in the real space becomes difficult as well.

Furthermore, conventional thermography visualization also disrupts the natural and smooth collaboration of multiple co-located people. Suppose that a discussion on the heat insulation design of an electrical device based on a displayed thermal image on a screen. In such a *screen collaboration*<sup>4</sup>, people are collaborating in front of the screen and often sitting side by side. Their attention is focused on the screen space, which is separate from the interpersonal communication space. As a result, the efficiency of the collaboration deteriorates.

To solve these problems with the conventional thermography visualization approach, we propose a novel approach where the captured thermal image is optically and simultaneously superimposed on the target object in real space through video projection. Because the thermal image emerges directly on the physical surfaces of the objects, and consequently the *object space* and *display space* are entirely matched, the observer can intuitively comprehend the heat distribution just in front of the target objects (Fig. 1(b)). Furthermore, the proposed approach makes possible *face-to-face collaboration* where multiple co-located people discuss the thermal properties of the target object placed between them. It has been indicated that *face-to-face collaboration* is more efficient than the aforementioned *screen collaboration* [3]. In *face-to-face collaboration*, people interact around a work space where communication cues such

---

<sup>4</sup>A collaboration performed based on information displayed on a screen

as gaze, gesture, and other nonverbal behaviors can be shared. Collaborators can see each other and the shared communication cues simultaneously.

The remainder of the paper is organized as follows. Related studies are briefly described in the subsequent section. Section 3 presents the detailed method of optical thermography superimposition with projected imagery. Section 4 describes the detailed implementation of the proposed system and proof-of-concept experiments to validate the usefulness of the proposed visualization method. Section 5 discusses the advantages and limitations of the proposed approach. Section 6 concludes the paper with directions for future work.

## 2. Related Work

Projection-based mixed reality (MR) is an emerging technology that merges real and virtual worlds by projecting computer-generated graphics onto a physical object to change (or augment) its appearance [4]. The following two technological issues must be addressed: geometric registration and radiometric compensation of the projection images. Once the projection image is geometrically registered to the object, a desired position on the object can be lit by a projector. The radiometric compensation technique cancels colors and textures on the object's surface; thus, a desired color can be displayed on the surface with a projected pixel. Note that the radiometric compensation technique only deals with the visible spectrum, not the LWIR light.

In recent years, several researchers have focused on projector-camera systems (ProCams) to address these issues through geometric and radiometric calibrations in which the visible camera captures the projected calibration patterns [5]. However, little research has focused on a projector and IR camera configuration such as [6]. Because an IR camera is sensitive only to thermal information and cannot capture projected calibration patterns, conventional calibration techniques cannot be directly applied to such a configuration.

*Veinviewer* is a commercially available ProCam where a captured near IR (NIR) image of a forearm is projected back onto it [7]. As a result, veins of the forearm are visually enhanced and a doctor can easily find a vein for an injection. The system consists of an NIR camera and a projector whose optical axes are coaxial with a dichroic mirror. This configuration enables the system to consistently project a geometrically registered image onto a forearm irrespective of its shape, position, and pose. However, this research does not deal with a LWIR camera, and radiometric compensation of the projection image is not considered.

Iwai and Sato proposed visualizing thermal information using video projection [8]. Their system detects a heated (or cooled) area on a paper screen from a captured thermal image and projects a uniform color on this area. Because their object is limited to a thin screen and they focus only on an interactive painting application, their approach is not applicable for other serious visualization purposes. In addition, they do not argue the geometric registration and radiometric compensation techniques.

This paper presents geometric registration and radiometric compensation techniques for a projector and IR camera configuration. The techniques are developed to realize thermography visualization that enables an observer to intuitively understand the heat distribution of the target object's surface.

### 3. Infrared Thermography Projection System

This paper proposes a novel thermography visualization approach in which the heat distribution of the target object's surface emerges directly on its surface in real space. Because the *object space* and *display space* are entirely matched on the physical object, the observer can intuitively comprehend the heat information.

This section describes details of the proposed visualization approach. First, the system configuration and process flow are explained. Then the geometric registration and radiometric compensation techniques applied to the system are introduced.

#### 3.1. System Configuration and Process Flow

Figure 2 shows the proposed system configuration and process flow. The system consists of an IR camera, a video projector, and a personal computer (PC) on which an image processing is performed. The first step of the process is visual enhancement of a captured thermal image of the target object. Any image enhancement algorithms (e.g., false color conversion) can be applied to a raw grayscale image. Second, the enhanced thermal image is geometrically registered to the object. The final projection image is then generated through radiometric compensation to display the desired color on the object's surface. Finally, the generated image is projected back onto the surface.

This section introduces the proposed geometric registration and radiometric compensation techniques. We apply two different combinations of techniques to different types of configurations. The first configuration is denoted as *non-coaxial* in which the optics of the projector and the IR camera are not coaxial. The second

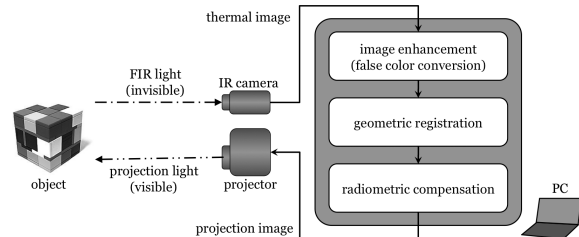


Figure 2: Overview of the proposed system

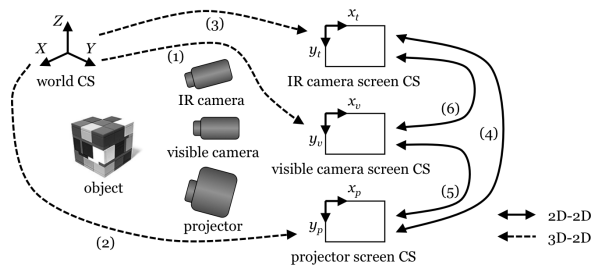


Figure 3: Coordinate systems of the *non-coaxial* configuration (CS: coordinate system)

configuration is denoted as *coaxial* in which the optics are coaxial.

#### 3.2. Geometric Registration

This section describes two types of geometric registration techniques.

##### 3.2.1. Not Coaxial Projector and IR Camera

We provide a geometric registration method for a configuration where the projector and the IR camera are arbitrarily placed and directed to the target object. The method requires the object's surface shape for determination of the correct image to project. Graycode pattern projection method [9] is applied for shape measurement as well as geometric calibration of the devices. An additional visible camera is integrated into the system to capture projected patterns that cannot be sensed by the IR camera. Figure 3 shows all the coordinate systems of the configuration: a world coordinate system (3D), an IR camera screen coordinate system (2D), a visible camera screen coordinate system (2D), and a projector screen coordinate system (2D).

Suppose that a 3D point  $(X, Y, Z)$  in a world coordinate system is projected onto a 2D image plane  $(x, y)$  as shown in Fig. 4. According to the pinhole camera model, the projection can be described by the perspective equation with the  $3 \times 4$  projection matrix  $C$ :

$$h \begin{bmatrix} x & y & 1 \end{bmatrix}^t = C \begin{bmatrix} X & Y & Z & 1 \end{bmatrix}^t, \quad (1)$$

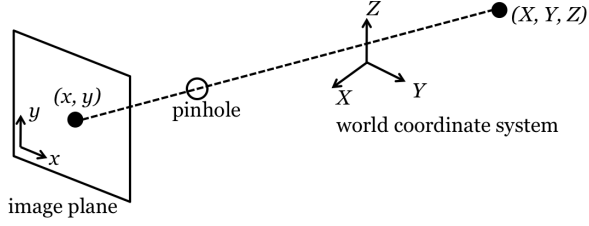


Figure 4: Pinhole camera model

where

$$\mathbf{C} = \begin{bmatrix} C_{11} & C_{12} & C_{13} & C_{14} \\ C_{21} & C_{22} & C_{23} & C_{24} \\ C_{31} & C_{32} & C_{33} & 1 \end{bmatrix}. \quad (2)$$

The projection matrix  $\mathbf{C}$  is determined up to a scale factor  $h$ . In our case, there are three unknown projection matrices ( $\mathbf{C}_v$  for the visible camera,  $\mathbf{P}$  for the projector, and  $\mathbf{C}_t$  for the IR camera) which have to be calibrated. Our geometric calibration is based on the DLT (Direct Linear Transformation) method [10, 11]. The projection matrix  $\mathbf{C}$  has eleven unknown parameters as shown in Eq. (2). Because two equations are derived from Eq. (1):

$$x = \frac{C_{11}X + C_{12}Y + C_{13}Z + C_{14}}{C_{31}X + C_{32}Y + C_{33}Z + 1}, \quad (3)$$

$$y = \frac{C_{21}X + C_{22}Y + C_{23}Z + C_{24}}{C_{31}X + C_{32}Y + C_{33}Z + 1}, \quad (4)$$

the unknown parameters of  $\mathbf{C}$  can be solved using a least-squares method with six or more correspondences between the 3D world coordinate system and the 2D screen coordinate system.

Lens distortion of the devices is not taken into account in the DLT method. However, lens distortion degrades the accuracy of the geometric registration only at the image periphery. Furthermore, our proposed system is an interactive on-site visualization system in which a user can rearrange the devices. When the user would like to check heat distribution of an area of the object's surface where the projection image is not well registered because of lens distortion, the proposed system allows the user to adjust the projector so that the image center directs at the interest part of the surface and recalibrate the system. If the user would like to improve the accuracy of the geometric registration, the data acquired through the calibration process can also be used to calibrate the lens distortion parameters that will be applied to lens distortion compensation [12, 13].

In the calibration process, we position a reference cube (160 [mm] on a side) with spatially-known feature points within the intersection of view frusta of the

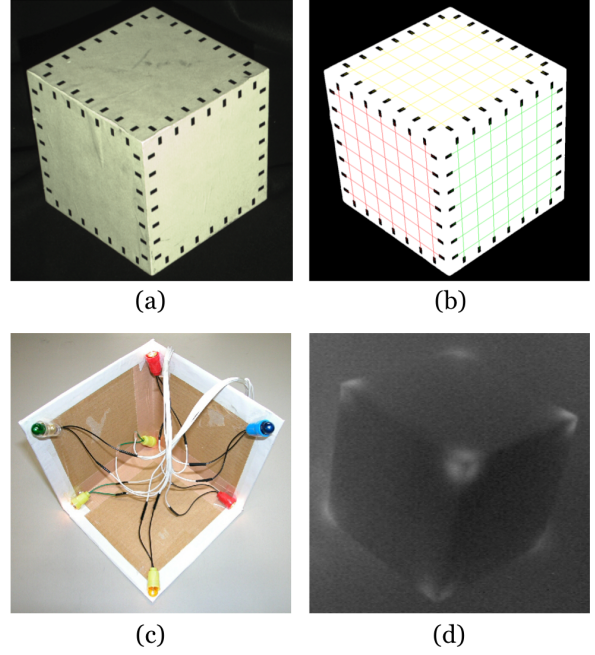


Figure 5: A fiducial cube: (a) a view of cube, (b) light bulbs attached on the cube, and (c) a captured thermal image of the cube while the light bulbs are lit

projector, the IR camera, and the visible camera. The fiducial cube determines the world coordinate system (Fig. 5(a)). Because the accuracy of the calibration results depends on the size of the cube on each image plane, we position the cube so that it is mapped onto each image plane as large as possible. Furthermore, a problem arises when the 3D points that are visible from each device are co-planar. In this case, the least-squares method degenerates due to the depth-scale ambiguity of viewing planar points. This means that there exists a family of solutions. To develop a unique solution in this case, the cube has to be placed so that at least two sides are visible from all the devices.

First, the visible camera captures the fiducial cube, and the fiducial points are automatically extracted in the captured image. Then, intersection points of two grid line segments each of which connects two fiducial points are calculated as shown in Fig. 5(b). The number of the intersection points is 147 in total. With 147 correspondences between the world coordinate system and the visible camera screen coordinate system,  $\mathbf{C}_v$  is calculated using a least-squares method (Fig. 3(1)). Once  $\mathbf{C}_v$  is determined, an arbitrary world coordinate value  $(X, Y, Z)$  can be converted to the corresponding visible camera screen coordinate value  $(x_v, y_v)$  by the following

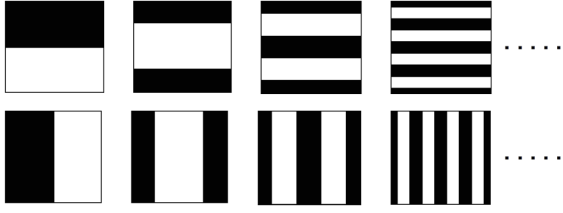


Figure 6: Horizontal (upper) and vertical (lower) graycode patterns

equation:

$$h \begin{bmatrix} x_v & y_v & 1 \end{bmatrix}^t = \mathbf{C}_v \begin{bmatrix} X & Y & Z & 1 \end{bmatrix}^t. \quad (5)$$

We apply the DLT method for the projector calibration because projector can also be modeled with the pin-hole camera model. First, horizontal and vertical graycode patterns (totally 20 patterns) are projected onto the fiducial cube (Fig. 6). The projected scenes are captured by the visible camera (Fig. 7). The captured images are processed and correspondences between visible camera screen and projector screen coordinate values are obtained. Correspondences between world and visible camera screen coordinate values were already obtained in the visible camera calibration. Therefore, correspondences between world and projector screen coordinate values are derived from these two correspondences. With the 147 correspondences, the projection matrix of the projector  $\mathbf{P}$  is calculated.  $\mathbf{P}$  is a  $3 \times 4$  matrix and converts arbitrary world coordinate values to the corresponding projector screen coordinate values  $(x_p, y_p)$  with the following equation (Fig. 3(2)).

$$h \begin{bmatrix} x_p & y_p & 1 \end{bmatrix}^t = \mathbf{P} \begin{bmatrix} X & Y & Z & 1 \end{bmatrix}^t. \quad (6)$$

To assess the accuracy of the calibration method, we mapped 3D world coordinate values of the intersection points onto the projector's image plane based on Eq. (6) and projected them back onto the fiducial cube. In this experiment, we used a fiducial cube on which not only the fiducial points but also the grid line segments were printed. Figure 8 shows the result. Figure 8(a) shows the cube without projection. Figure 8(b) shows optical superimposition of the calculated intersection points by projected imagery. The mean distance of the projected points to the actual intersection points was less than 1.0 [mm].

The IR camera is calibrated with the same fiducial cube (Fig. 3(3)). Seven light bulbs are attached on the corners of the cube and warm them (Fig. 5(c)). Although the IR camera cannot detect the fiducial points, the corner can be found in the captured thermal image,

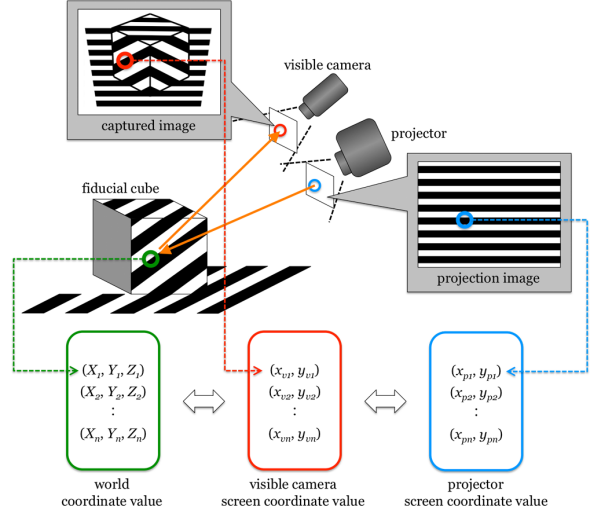


Figure 7: Graycode projection to obtain geometric correspondences between the world and the projector screen coordinate systems via visible camera screen coordinate system

as shown in Fig. 5(d). The corner positions in the IR camera screen coordinate system  $(x_t, y_t)$  are manually obtained from the captured IR camera image. Note that the user has to pay attention to the orientation of the cube. Each obtained IR camera coordinate value of a corner has to be correlated with the right world coordinate value. From the obtained 2D positions and the corresponding world coordinate values, a set of calibration parameters of the IR camera  $\mathbf{C}_t$  is calculated.  $\mathbf{C}_t$  is a  $3 \times 4$  matrix and converts arbitrary world coordinate values to IR camera screen coordinate values with the following equation.

$$h \begin{bmatrix} x_t & y_t & 1 \end{bmatrix}^t = \mathbf{C}_t \begin{bmatrix} X & Y & Z & 1 \end{bmatrix}^t. \quad (7)$$

Finally, the fiducial cube is replaced with the target object. The graycode patterns are projected again onto it and the projected scene is captured by the visible camera. Its shape, or world coordinate value, is measured through triangulation. Then, pixel correspondences among the visible camera screen, IR camera screen, and projector screen coordinate systems are calculated with the calibration parameters and the measured world coordinate value. The correspondences are stored as look-up tables (Fig. 3(4), (5), (6)).

The shape has to be measured again when the object is moved. Because graycode pattern projection generally takes about a few seconds, this method cannot be applied to moving objects.

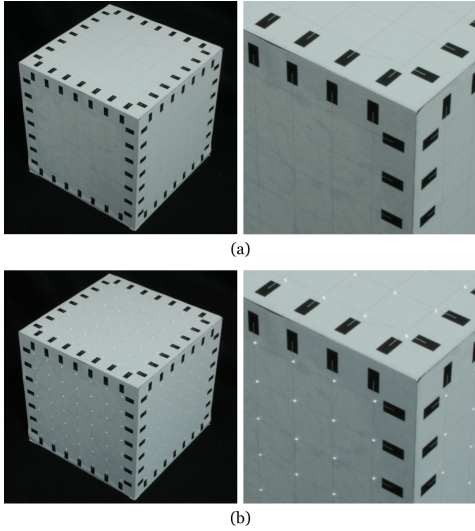


Figure 8: Optical superimposition of the calculated intersection points on a fiducial cube by projected imagery (right: magnified view): (a) the cube on which grid line segments are printed, (b) projection result

### 3.2.2. Coaxial Projector and IR Camera

A simpler geometric registration method can be applied when the optics of the projector and the IR camera are coaxial. In this case, no visible camera is required. After a single off-line geometric calibration, the geometry remains correct even as the target object moves or the environment changes. Therefore, this method does not have to assume the surface shape to be known. This is particularly useful for a dynamic scene.

The optical axes of the projector and the IR camera are aligned by a dichroic mirror, as shown in Fig. 9. A previous study applied a homography transformation to register coaxial visible and IR cameras [14]. A homography is an invertible transformation from a projective plane to another projective plane. We also apply homography to the projector and IR camera registration. The  $3 \times 3$  homography matrix is calculated with more than four corresponding positions between the projector screen and the IR camera screen coordinate systems.

More than four light bulbs are placed on a planar surface and captured by the IR camera. Their positions in the captured thermal image are obtained manually. Corresponding projector screen coordinate values are also manually obtained. From these correspondences, a homography matrix is calculated. With the homography matrix  $\mathbf{H}$ , an IR camera screen coordinate value  $(x_t, y_t)$  is converted to a projector screen coordinate value  $(x_p, y_p)$ .

$$h \begin{bmatrix} x_p & y_p & 1 \end{bmatrix}^t = \mathbf{H} \begin{bmatrix} x_t & y_t & 1 \end{bmatrix}^t. \quad (8)$$

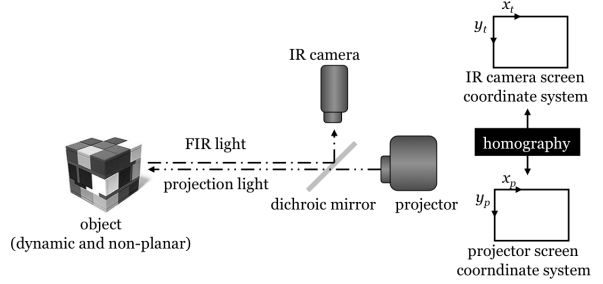


Figure 9: Coordinate systems of the coaxial configuration

### 3.3. Radiometric Compensation

In the real world, most objects have spatially varying reflectance properties that disturb the appearance of a projected image. We apply a radiometric compensation method [15], so as not to decrease the visibility of the appearance content of the projected thermal image. This method can be applied to a static scene only. Thus, the object's surface colors can be canceled in the *non-coaxial* case.

The method uses the visible camera of the system shown in Fig. 3 to obtain an affine correlation in color space between the projection and the result captured by the camera for each camera pixel. This affine correlation can transform the desired color appearance on a physical object's surface into a projected color value. When the input RGB value for the projector is represented as  $(R_p, G_p, B_p)$  and the captured RGB value of the visible camera is represented as  $(R_c, G_c, B_c)$ , the correlation between them can be represented by the following equation in the affine transformation.

$$\begin{bmatrix} R_p & G_p & B_p \end{bmatrix}^t = \mathbf{K} \begin{bmatrix} R_c & G_c & B_c & 1 \end{bmatrix}^t. \quad (9)$$

$\mathbf{K}$  is a  $3 \times 4$  matrix that transforms a camera's color space to that of a projector. Therefore,  $\mathbf{K}$  is called a color mixing matrix that takes into account the projector's spectral characteristics, the camera's spectral sensitivity, and the spectral reflectance of the object's surface.  $\mathbf{K}$  has to be calibrated for each camera pixel. Once at least four correspondences between  $(R_c, G_c, B_c)$  and  $(R_p, G_p, B_p)$  are obtained,  $\mathbf{K}$  is calculated by a least-squares method. In the calibration process, more than four simple color patterns (e.g., red, green, blue, yellow, magenta, and cyan) are projected and the reflectance of each projected pattern is captured. After this color calibration, images of the desired color can be displayed on surfaces under consideration of their reflectance. The color of the compensated projection image is calculated by Eq. (9) for each pixel of the projection image.

As described above, the color mixing matrix  $\mathbf{K}$  can be calibrated without any prior information about the spectral characteristics of the projector, the camera, and the object's surface.  $\mathbf{K}$  is unique for the given setup of the projector-camera system. Therefore  $\mathbf{K}$  has to be recalibrated whenever even one of the devices (the projector, the camera, and the object) is replaced or translated, or the environment light is changed. Because more than four color patterns have to be projected in each calibration, this radiometric compensation cannot be applied to a moving object. Fujii et al. proposed a radiometric compensation method that accounts for a moving object [16]. However, this method is quite sensitive to noise in a captured image, and thus cannot be used in a practical application.

#### 4. Proof-of-Concept Experiments

This section describes proof-of-concept experiments to validate the proposed visualization method. First, detailed information about the experimental systems is provided. Then two basic experiments are explained, which are conducted to validate the proposed geometric registration and radiometric compensation techniques. Finally, four application examples are shown to confirm the method's feasibility.

##### 4.1. Experimental System

Figure 10 shows two different experimental setups for the *non-coaxial* and *coaxial* cases. The same equipment (an IR camera (Mitsubishi IR-SC1<sup>5</sup>), a visible camera (Tokyo Electronic Industry CS5850), and a projector (NEC MT1075J)) are used in both systems. These devices are connected to a PC (CPU: Intel Pentium4 2.5 [GHz]) that controls them. The *coaxial system* applies a dichroic mirror that reflects IR light and transmits visible light. The input-output characteristics of both the visible camera and the projector are linearized in advance.

##### 4.2. Basic Experiments

Two experiments are conducted to validate the proposed geometric registration and radiometric compensation techniques. A cup (40 [mm] radius and 95 [mm] height) into which hot water (60 [°C]) is poured is used as a target object in the experiments. The surface of the cup has spatially varying reflectance properties.

<sup>5</sup>wavelength range: 8-12[ $\mu\text{m}$ ], image resolution: 320x240 [pixel], frame rate: 30 [fps] (from the specification sheet of the product)

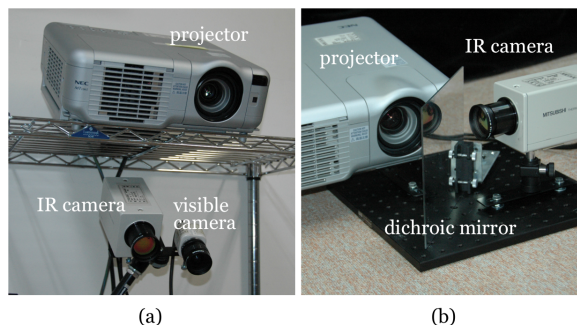


Figure 10: Experimental setups: (a) the *non-coaxial system* and (b) the *coaxial system*

##### 4.2.1. Non-Coaxial System

Experimental results for the *non-coaxial system* are shown in Fig. 11. Figure 11(a) shows the appearance of the object under environment light captured by the system's visible camera. Figure 11(b) shows the heat distribution of the object's surface captured by the IR camera. Figure 11(c) shows the generated heat distribution from the perspective of the visible camera. This conversion is accomplished on the basis of the look-up table of pixel correspondences between the IR camera screen and the visible camera screen coordinate systems. This image is the target appearance displayed on the object.

The target image is geometrically converted to an image viewed from the perspective of the projector. Then the color of the projection image is modified through the radiometric compensation (Fig. 11(d)). Figure 11(e) is the projection result captured by the visible camera. A result where the projection image is not radiometrically compensated is also prepared for comparison (Fig. 11(f)). The average RGB differences between the target appearance (Fig. 11(c)) and the final appearances are 69 (with radiometric compensation, Fig. 11(e)) and 116 (without radiometric compensation, Fig. 11(f))<sup>6</sup>.

##### 4.2.2. Coaxial System

Experimental results for the *coaxial system* are shown in Fig. 12, where the heat distribution is projected back onto the moving object. The frame rate of the projection was 30 [frame/sec]; thus, the system could superimpose the heat distribution in real time.

##### 4.3. Application Experiments

Four experiments were conducted to validate the feasibility of the proposed thermography visualization method. The *coaxial system* was used for all the experiments.

<sup>6</sup>The camera pixel value ranges from 0 to 255.

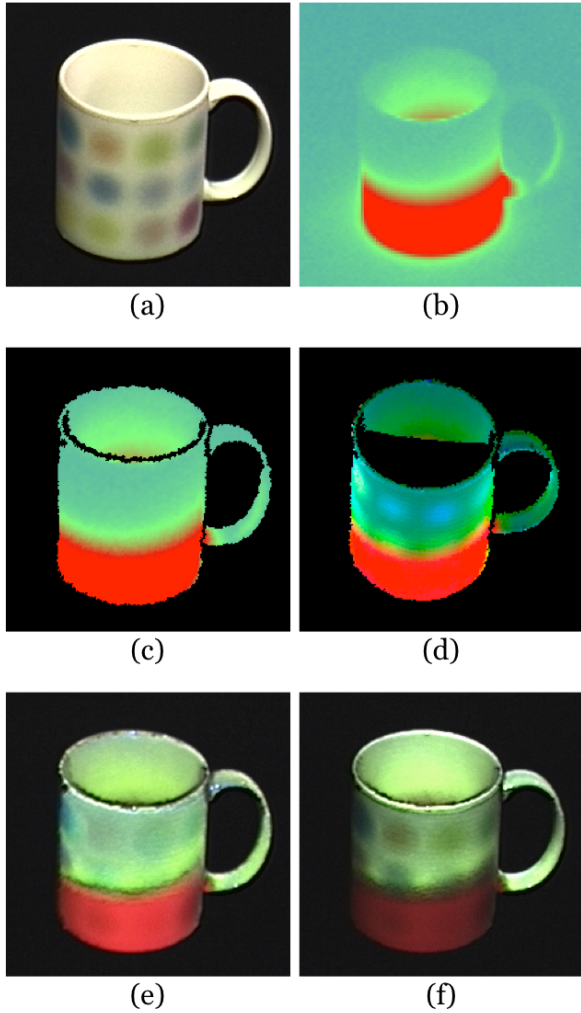


Figure 11: Experimental results of the *non-coaxial system*: (a) the object under environment light, (b) a captured thermal image, (c) the heat distribution from the visible camera perspective, (d) a projection image with the radiometric compensation, (e) a projection result with radiometric compensation, and (f) a projection result without the radiometric compensation

#### 4.3.1. Heat Observation of Cluttered Scene

In conventional thermography visualization, it is difficult for an observer to find the physical location of the target object that has a unique temperature in a cluttered scene. The experiment described here is conducted to show that the proposed method makes this task more intuitive for the observer. The object scene of the experiment is covered with many similar objects, specifically same-shaped paint tubes. One tube is empty and the others are filled with paint.

Figure 13(a) shows the appearance of the tubes under environment light. Figure 13(b) shows a thermal



Figure 12: Experimental results for the coaxial system

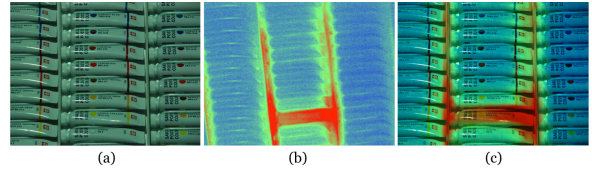


Figure 13: Experimental results for a cluttered scene: (a) paint tubes under environment light, (b) a captured thermal image of the tubes, and (c) the projection result

image of the tubes after they are heated with a handy dryer. Due to different heat capacity, the tube that has a higher temperature is the one that is empty. Figure 13(c) shows the projection result. Because the heat distribution emerges directly on the tubes' surfaces, the observer can identify the empty tube in real space at a glance.

#### 4.3.2. Heat Observation of White Wall

Thermography is often used in NDT of a building. An observer points a thermal imager at a wall, ceiling, or floor to check the heat distribution. However, many surfaces in a building do not have complex texture. Therefore, the observer may face difficulty in finding geometric correspondences between the object in real space and the image displayed on the screen because it offers no visual clues. This experiment is conducted to show that the proposed visualization method is effective in such a case.

The object of the experiment is a wall under which steel frames are embedded (Fig. 14(a)). An air conditioner installed in a ceiling blows cold air at the wall. Because the steel frames conduct heat from the outside of the building, parts of the wall where the steel is embedded become warmer than other parts. Three frames can be found in the captured thermal image of the wall (Fig. 14(b)). Figure 14(c) shows the projection result. Because the heat distribution emerges directly on the wall's surface, the observer can comprehend the positions of the steel frames in real space at a glance.

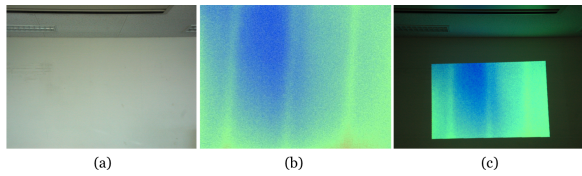


Figure 14: Experimental results for a white wall: (a) the wall under environment light, (b) a captured thermal image of the wall, and (c) the projection result

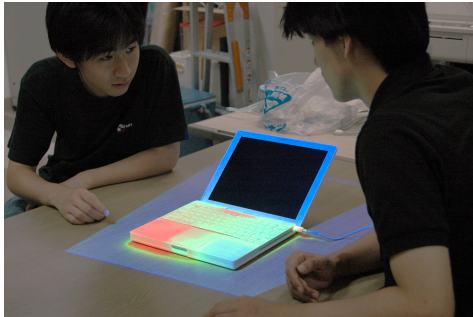


Figure 15: Experimental result for face-to-face cooperative heat observation of a notebook PC

#### 4.3.3. Heat Observation in Face-to-Face Collaboration

An example of face-to-face cooperative work using the proposed system is shown here. In the experiment, two observers sit at a table on which a notebook PC (Apple iBook G4) is placed, and discuss its heat design (Fig. 15). The heat distribution of the PC is projected onto its surface. The system allows the two observers to discuss the heat design of the PC while pointing at interesting parts and establishing eye contact.

#### 4.3.4. Heat Observation of Human Body

Thermography is widely used in medicine. A doctor uses a thermal image of a patient's body for diagnosis. Thermography screening is another important medical application. Body heat of travelers are monitored in an airport to check for people infected with a severe disease such as SARS or influenza.

Figure 16(a) shows a projection result of a participant's hand. Because the heat distribution emerges directly on the hand itself, a doctor can comprehend it in real space. Such direct visualization may aid the doctor's diagnosis. Furthermore, the system allows the doctor to talk about the diagnosis with the patient in face-to-face collaboration.

Figure 16(b) shows a result where heat distributions of participants' bodies are projected back onto them. The right participant looks to have low temperature on his face compared to the left participant. This is be-



Figure 16: Experimental results for human bodies: (a) a hand and (b) multiple people

cause that the right participant sweats although the other does not. This example is a simulation of thermography screening in an airport. The system allows the examiners of thermography screening to find and identify an infected person at a glance.

## 5. Discussion

The results of the basic experiments shown in 4.2 validate the proposed geometric registration and radiometric compensation techniques. It can be seen that the heat distributions are geometrically registered to the object's surface in real time even when it is moving (Fig. 12). Furthermore, it is shown in 4.2.1 that radiometric compensation can decrease the color difference between the target image and the final result (Fig. 11(e)(f)). However, radiometric compensation works only when the object is static.

As described in Sec. 1, an observer cannot intuitively comprehend the heat distribution of a cluttered scene or an object which does not have complex texture on its surface. The results shown in 4.3.1 and 4.3.2 confirm that the proposed approach realizes intuitive thermography visualization in such cases. In the proposed system, the heat distribution of the object's surface emerges directly on its surface. As a result, the observer can intuitively comprehend it even when there are many similarly shaped objects or no visual clues appear in the scene. Note that modern infrared thermography devices are often equipped with visible laser pointers that greatly ease target discrimination in cluttered environment. On the other hand, our method realizes another scientific visualization of heat distribution with a richer displaying technology. We believe that our proposed technique improves the user's effort on the discrimination task compared to the laser pointer by the projected richer heat information. Therefore, one of the future works would be to investigate and compare the usability of the proposed system and the laser pointer based system.

As noted in Sec. 1, a *screen collaboration* disrupts efficient cooperative work because the collaborators' attention is focused on the screen rather than on the object. The result in 4.3.3 shows that the proposed visualization system provides *face-to-face collaboration* in a cooperative heat observation. It is also indicated in Sec. 1 that plenty of nonverbal cues occur during communication in a *face-to-face collaboration*. These nonverbal cues promote active discussions. Therefore, the proposed visualization system realizes effective collaboration in a discussion on heat design. The proposed system is also useful in medical applications, as shown in 4.3.4. To summarize the application experiments, the proposed visualization approach is feasible in many application fields.

## 6. Conclusion and Future Work

This paper presents a novel thermography visualization method in which the heat distribution of the target object's surface emerges directly on the object in real space. This is accomplished by the optical superimposition of the captured thermal image on the object's surface through video projection. The proposed method applies geometric registration and radiometric compensation to the thermal image in order to generate a projection image. Basic experiments are conducted to validate the proposed geometric registration and radiometric compensation techniques. In addition, application experiments confirm the intuitiveness, effectiveness, and feasibility of the proposed visualization approach.

One goal of future work is to develop a robust radiometric compensation method for a moving object to make the system more widely applicable. Because both projector and IR camera are currently becoming smaller, another future project is to build a mobile system with mobile devices and investigate its usability and appropriate applications.

## References

- [1] S.G. Burnay, T.L. Williams, and C.H.N. Jones. *Applications of Thermal Imaging*. Adam Hilger, 1988.
- [2] Herbert Kaplan. *Practical Applications of Infrared Thermal Sensing and Imaging Equipment (Tutorial Texts in Optical Engineering)*. Society of Photo Optical, 2007.
- [3] Mark Billinghurst, Hirokazu Kato, Kiyoshi Kiyokawa, Daniel Belcher, and Ivan Poupyrev. Experiments with Face-To-Face Collaborative AR Interfaces. *Virtual Reality*, 6(3):107–121, 2002.
- [4] Oliver Bimber and Ramesh Raskar. *Spatial Augmented Reality: Merging Real and Virtual Worlds*. A. K. Peters Ltd., 2005.
- [5] Oliver Bimber, Daisuke Iwai, Gordon Wetzstein, and Anselm Grundhöfer. The Visual Computing of Projector-Camera Systems. *Computer Graphics Forum*, 27(8):2219–2254, 2008.
- [6] Hideki Koike, Yoichi Sato, and Kobayashi Yoshinori. Integrating Paper and Digital Information on EnhancedDesk: A Method for Realtime Finger Tracking on an Augmented Desk System. *ACM Transactions on Computer-Human Interaction*, 8(4):307–322, December 2001.
- [7] Herbert D. Zeman, Gunnar Lovhoiden, and Carlos Vrancken. Prototype Vein Contrast Enhancer. *SPIE Optical Engineering*, 44(8):086401 (9 pages), 2005.
- [8] Daisuke Iwai and Kosuke Sato. Heat Sensation in Image Creation with Thermal Vision. In *Proceedings of ACM International Conference on Advances in Computer Entertainment Technology (ACE)*, pages 213–216, 2005.
- [9] Kosuke Sato and Seiji Inokuchi. Range-Imaging System Utilizing Nematic Liquid Crystal Mask. In *Proceedings of IEEE International Conference on Computer Vision (ICCV)*, pages 657–661, 1987.
- [10] Y. I. Abdel-Aziz and H. M. Karara. Direct Linear Transformation from Comparator Coordinates into Object Space Coordinates in Close-Range Photogrammetry. In *Proceedings of the Symposium on Close-Range Photogrammetry*, pages 1–18, 1971.
- [11] Olivier Faugeras. *Three-Dimensional Computer Vision : A Geometric Viewpoint*. MIT Press, 1993.
- [12] Roger Y. Tsai. A versatile Camera Calibration Technique for High-Accuracy 3D Machine Vision Metrology Using Off-the-Shelf TV Cameras and Lenses. *IEEE Journal of Robotics and Automation*, RA-3(4):323–344, August 1987.
- [13] Zhengyou Zhang. A Flexible New Technique for Camera Calibration. *IEEE Transactions on Pattern Analysis and Machine Intelligence (PAMI)*, 22(11):1330–1334, November 2000.
- [14] Kazutaka Yasuda, Takeshi Naemura, and Hiroshi Harashima. Thermo-Key: Human Region Segmentation from Video. *IEEE Computer Graphics and Applications*, 24(1):26–30, 2004.
- [15] Takenobu Yoshida, Chinatsu Horii, and Kosuke Sato. A Virtual Color Reconstruction System for Real Heritage with Light Projection. In *Proceedings of International Conference on Virtual Systems and MultiMedia (VSMM)*, pages 825–831, 2003.
- [16] Kensaku Fujii, Michael D. Grossberg, and Shree K. Nayar. A Projector-Camera System with Real-Time Photometric Adaptation for Dynamic Environments. In *Proceedings of IEEE Conference on Computer Vision and Pattern Recognition (CVPR)*, volume 1, pages 814–821, 2005.